NDUFB8 Mutations Cause Mitochondrial Complex I Deficiency in Individuals with Leigh-like Encephalomyopathy

Dorota Piekutowska-Abramczuk,[1,12] Zahra Assouline,[2,12] Lavinija Mataković,[3] René G. Feichtinger,[3] Eliška Koňařiková,[4,5] Elżbieta Jurkiewicz,[6] Piotr Stawiński,[7,8] Mirjana Gusic,[4,5] Andreas Koller,[3] Agnieszka Pollak,[8] Piotr Gasperowicz,[7] Joanna Trubicka,[1] Elżbieta Ciara,[1] Katarzyna Iwanicka-Pronicka,[9] Dariusz Rokicki,[10] Sylvain Hanein,[11] Saskia B. Wortmann,[3,4,5] Wolfgang Sperl,[3] Agnès Rötig,[11] Holger Prokisch,[4,5] Ewa Pronicka,[1,10,13] Rafał Płoski,[7,13,*] Giulia Barcia,[2,13] and Johannes A. Mayr[3,13,*]

Respiratory chain complex I deficiency is the most frequently identified biochemical defect in childhood mitochondrial diseases. Clinical symptoms range from fatal infantile lactic acidosis to Leigh syndrome and other encephalomyopathies or cardiomyopathies. To date, disease-causing variants in genes coding for 27 complex I subunits, including 7 mitochondrial DNA genes, and in 11 genes encoding complex I assembly factors have been reported. Here, we describe rare biallelic variants in *NDUFB8* encoding a complex I accessory subunit revealed by whole-exome sequencing in two individuals from two families. Both presented with a progressive course of disease with encephalo(cardio)myopathic features including muscular hypotonia, cardiac hypertrophy, respiratory failure, failure to thrive, and developmental delay. Blood lactate was elevated. Neuroimaging disclosed progressive changes in the basal ganglia and either brain stem or internal capsule. Biochemical analyses showed an isolated decrease in complex I enzymatic activity in muscle and fibroblasts. Complementation studies by expression of wild-type *NDUFB8* in cells from affected individuals restored mitochondrial function, confirming *NDUFB8* variants as the cause of complex I deficiency. Hereby we establish *NDUFB8* as a relevant gene in childhood-onset mitochondrial disease.

Respiratory chain complex I (CI; NADH:ubiquinone oxidoreductase), one of the largest membrane-bound protein complexes in the human cell, is essential for oxidative energy metabolism as it powers ATP synthesis by using the reducing potential of NADH to proton translocation across the inner mitochondrial membrane. Mammalian complex I is composed of 44 different subunits including 14 highly conserved (from bacteria to humans) core subunits and their 9 cofactors (a flavin mononucleotide [FMN] and eight iron-sulfur [Fe-S] clusters) that house the catalytic machinery. Seven subunits (encoded by *NDUFS1* [MIM: 157655], *NDUFS2* [MIM: 602985], *NDUFS3* [MIM: 603846], *NDUFS7* [MIM: 601825], *NDUFS8* [MIM: 602141], *NDUFV1* [MIM: 161015], and *NDUFV2* [MIM: 600532]) are hydrophilic proteins encoded by nuclear genes while the remaining (encoded by *MT-ND1* [MIM: 516000], *MT-ND2* [MIM: 516001], *MT-ND3* [MIM: 516002], *MT-ND4* [MIM: 516003], *MT-ND4L* [MIM: 516004], *MT-ND5* [MIM: 516005], and *MT-ND6* [MIM: 516006]) are hydrophobic membrane-bound proteins, encoded by the mitochondrial genome. The conserved core subunits are organized in three functional domains for NADH oxidation (N), for ubiquinone reduction (Q), and for proton translocation (P).[1] In addition, approximately 30 nuclear-encoded accessory subunits arranged around a core are essential for structure and stability of the complex.[2–4] Moreover, functionally active complex I requires the concerted action of at least 12 assembly factors.[2,3] Complex I is organized in supercomplexes together with other respiratory chain enzymes. The most abundant supercomplex consists of one molecule of complex I, two molecules of complex III, and one molecule of complex IV ($CI_1III_2IV_1$) and is termed respirasome. However, higher organized supra-supercomplexes, like $CI_2III_2IV_2$, have also been reported.[5–7]

Isolated complex I deficiency (MIM: 252010) appeared the most frequently identified biochemical defect in childhood mitochondrial disease (MD), accounting for 20%–30% of cases.[8,9] Clinical symptoms include fatal infantile lactic acidosis, cardiomyopathy, encephalopathy, myopathy, and hepatopathy. Leigh syndrome (MIM: 256000) and Leber hereditary optic neuropathy (LHON [MIM: 535000]) are syndromes frequently associated with complex I deficiency.[8]

[1]Department of Medical Genetics, The Children's Memorial Health Institute, 04-730 Warsaw, Poland; [2]Department of Genetics, Hôpital Necker-Enfants-Malades, 75015 Paris, France; [3]Department of Pediatrics, Salzburger Landeskliniken and Paracelsus Medical University Salzburg, 5020 Salzburg, Austria; [4]Institute of Human Genetics, Helmholtz Zentrum München - German Research Center for Environmental Health, 85764 Neuherberg, Germany; [5]Institute of Human Genetics, Technische Universität München, 81675 Munich, Germany; [6]Department of Diagnostic Imaging, The Children's Memorial Health Institute, 04-730 Warsaw, Poland; [7]Department of Medical Genetics, Warsaw Medical University, 02-106 Warsaw, Poland; [8]Department of Genetics, Institute of Physiology and Pathology of Hearing, 05-830 Warsaw/Kajetany, Poland; [9]Department of Audiology and Phoniatrics, The Children's Memorial Health Institute, 04-730 Warsaw, Poland; [10]Department of Paediatrics, Nutrition and Metabolic Diseases, The Children's Memorial Health Institute, 04-730 Warsaw, Poland; [11]INSERM U1163, Université Paris Descartes-Sorbonne Paris Cité, Institut Imagine, 75015 Paris, France
[12]These authors contributed equally to this work
[13]These authors contributed equally to this work
*Correspondence: rploski@wp.pl (R.P.), h.mayr@salk.at (J.A.M.)
https://doi.org/10.1016/j.ajhg.2018.01.008.

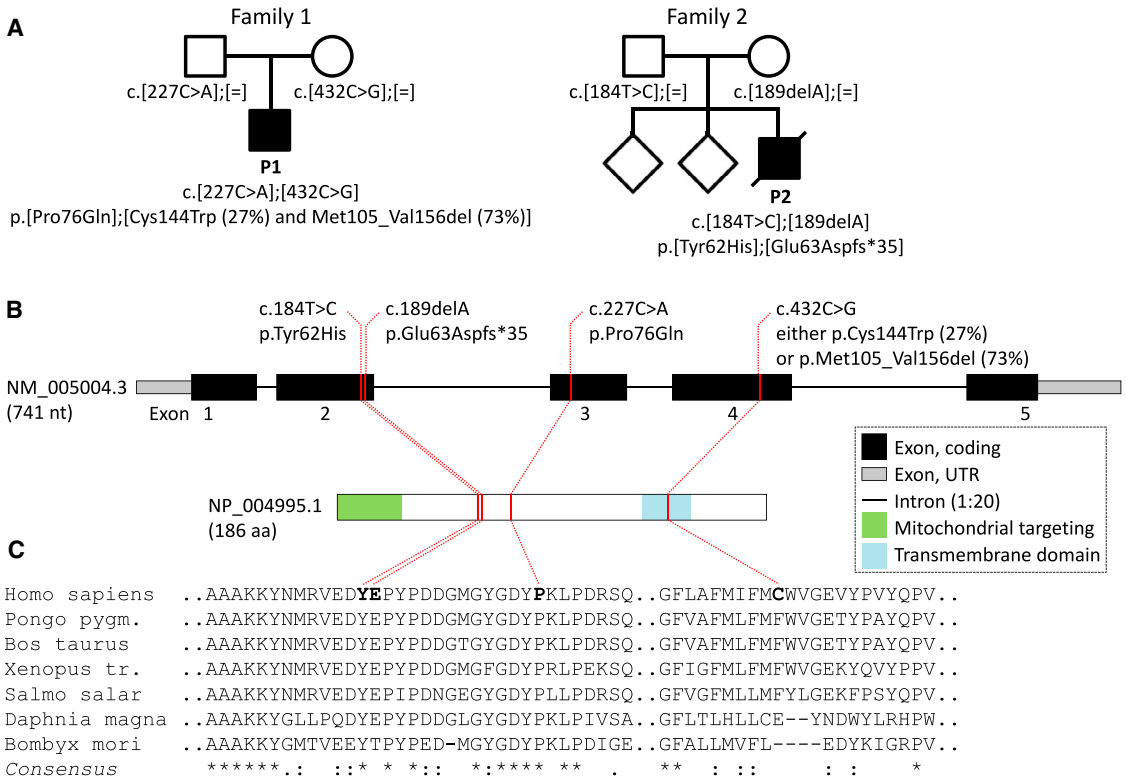

Figure 1. Mutations Identified in *NDUFB8* in Two Families
(A) Compound heterozygous *NDUFB8* mutations identified in two families.
(B) Gene structure of *NDUFB8* and localization of mutations.
(C) Multiple alignment of NDUFB8 protein sequences from different species by Clustal Omega.

To date, mutations have been reported in 27 complex I subunits including all 7 mitochondrial DNA (mtDNA)-encoded subunits, 7 nuclear DNA-encoded core and 13 nuclear DNA-encoded accessory subunits, and in addition in 11 assembly factors.[10,11] The emerging use of whole-exome sequencing (WES) has become an essential tool in identification of the heterogeneous molecular background of complex I deficiency and discovery of novel disease genes underlying this condition.[12,13]

The study was conducted according to the principles of the Helsinki Convention. The study protocol was approved by local institutional bioethics commissions in Warsaw and Paris. Parental informed consent was given for biochemical and molecular analyses.

We investigated two affected individuals (P1, P2) from two unrelated families (Figure 1). Pregnancy and birth were unremarkable. At the age of 3 and 6 months, respectively, first symptoms were noted including failure to thrive, low consciousness, muscular hyoptonia, and seizures (in one). Lactate was elevated in plasma and cerebrospinal fluid. Brain MRI showed abnormal signal intensities in the basal ganglia and brain stem as they are typically found in individuals with Leigh syndrome (Figure 2). P1 developed hypertrophy of the left cardiac ventricle. P2 died at the age of 15 months, and P1 is alive at the age of 6 years. Detailed case reports can be found in the Supplemental Note.

The activity of respiratory chain enzymes in homogenate of muscle tissue of P1 revealed isolated complex I deficiency (5.0% of citrate synthase [CS] activity, reference range > 6.7%). The activity of complex I was reduced in fibroblasts of P2 (7 nmol/min/mg protein, ref. 20.1–53.7) while cytochrome *c* oxidase (301 nmol/min/mg protein, ref. 62–139) and citrate synthase (99 nmol/min/mg protein, ref. 51–96) were elevated. Blue native gel electrophoresis performed with protein from muscle homogenates of P2 revealed decreased amount of complex I protein, and the other respiratory chain complexes were present in normal amount or slightly reduced, like cytochrome *c* oxidase (Figure 3A). Blue native gel electrophoresis also showed a specific decrease of complex I in a muscle biopsy sample of P1 (Figure S1). Oxygen consumption rates were decreased in digitonin-permeabilized fibroblasts of P2 with the substrates malate+glutamate 1.7 nmol O_2/min/mg protein (ref. 4.7–11.7) but normal with succinate 16.3 nmol O_2/min/mg protein (ref. 10.0–20.3) and glycerol-3-phosphate 10.3 nmol O_2/min/mg protein (ref. 5.2–10.6).[14]

Whole-exome sequencing was performed in P1 using DNA from peripheral blood and TruSeq Exome Enrichment Kit methodology (Illumina) followed by high-throughput sequencing on HiSeq 1500 and read alignment to the human genome (UCSC Genome Browser build hg19).[15] Mitochondrial and nuclear genomes were

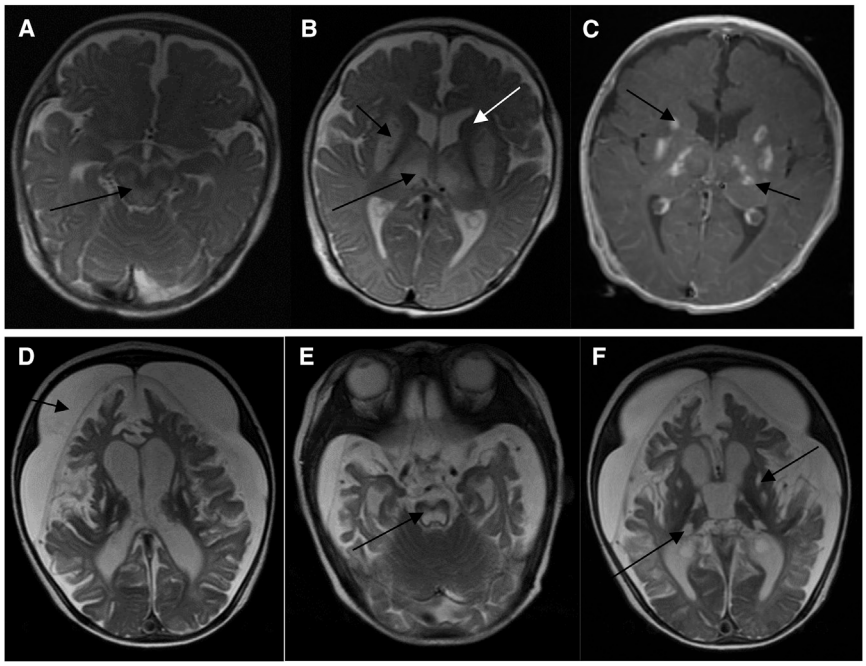

Figure 2. Brain Magnetic Resonance Imaging in Individual P1
Top row: MR brain examination at the age of 3 months; axial T2-weighted images; symmetrical increased signal intensity in the midbrain (A, black arrow), bilateral putamina and thalami (B, black arrows), sparing of the caudate heads (B, white arrow). Axial post contrast T1-weighted image (C, black arrows); patchy putamina and thalami enhancement.
Bottom row: follow-up MRI at the age of 6 months: profound supratentorial brain and brainstem atrophy with large bilateral, chronic subdural hematomas (D, black arrow) and cystic lesions in the midbrain (E, black arrow) and in the bilateral putamina and thalami (F, black arrows).

sequenced simultaneously. Detected variants that passed quality control were prioritized based on inheritance model, allele frequency, pathogenicity prediction algorithms, and mutation database search. We considered variants predicted to modify protein function (splice site, nonsense, missense, indels) of minor allele frequency less than 0.01 (for AR inheritance) and 0.001 (for AD) in four databases (ExAC, 1000 Genomes, ESP6500, and in-house project of 2,000 exomes of Polish individuals with unrelated diseases).

The sequencing run achieved 83,924,076 reads and the 20-fold coverage was 94.4% yielding a total of 225,136 variants. Approximately 13,500 non-synonymous single-nucleotide variants (SNVs) were detected and subsequently filtered for variants with MAF < 0.1% in our in-house database and public databases, identifying 134 variants. Bi-allelic filtering resulted in identification of five genes including one with mitochondrial localization, *NDUFB8* (GenBank RefSeq: NM_005004.3; NP_004995.1; MIM: 602140), highly conserved among vertebrates. The conservation of orthologous sequences is lower in insects and other animals and rather poor in fungi and plants (Figure S2).

The missense mutation c.227C>A (p.Pro76Gln) was found in 1 out of 246,208 alleles in the gnomAD database, and the missense mutation c.432C>G (p.Cys144Trp) was found in neither public databases nor in 2,000 in-house exomes. The variants were confirmed by Sanger sequencing (Figure S3) and biallelic inheritance was confirmed by sequencing of parental DNA (data not shown).

Both nucleotide c.227 and amino acid at position 76 are highly conserved in numerous species (Figure 1), pointing to a likely pathogenic character of the identified variant; all used prediction algorithms assessed it as deleterious (Table S1). The second variant, c.432C>G (p.Cys144Trp) (Figure 1), disturbs a weakly conserved *NDUFB8* nucleotide as well as amino acid; large physicochemical difference between Cys and Trp allow us to consider it as likely pathogenic. It was assessed as deleterious by Mutation Assessor, Likelihood Ratio Test (LRT), and Mutation Taster algorithms, while Alamut analysis suggested possible splicing alterations. Investigation of the c.432C>G mutation by Human Splicing Finder (HSF) algorithm suggested creation of a new splice donor site by this mutation but also the generation of an exonic splicing silencer (ESS). In order to show potential consequences of this mutation on mRNA level, we isolated RNA from fibroblasts and prepared cDNA by reverse transcription using oligo-dT primers.[16] Quantitative real-time PCR was performed with a forward primer from the junction of exons 1 and 2 (5′-ACAGCCTCCCACATGACC-3′) and a reverse primer from the terminal exon 5 (5′-TTT CTAGGAATGAGGGAGTCCT-3′) amplifying a 534 bp fragment of the *NDUFB8* transcript. Compared to housekeeping transcripts (*HPRT1*, *RPL27*), the expression of *NDUFB8* was normal. However, an additional product was amplified with a size of approximately 380 bp in length. Sanger sequencing revealed that exon 4 was missing in the smaller product (Figure S4), indicating a splice defect due to the c.432C>G mutation. The products were labeled with a nested reverse primer located on the terminal exon 5 (5′-6-FAM-TCCTAGTTAGAGGA CCCAAAAGC-3′) by a single hot stop PCR cycle (96°C 1 min, 63°C 40 s, 72°C 30 s). Labeled products were separated by capillary electrophoresis (3500 Genetic Analyzer, Thermo). Quantification of undigested PCR products revealed 60% of the signal at 516 bp and 40% at 360 bp (Figure S5). In DNA from ten control fibroblasts, only very low amount (0.19% on average) of exon 4 skipping was observed by RNA-seq[10] (Figure S6), indicating that skipping of exon 4 in the *NDUFB8* transcript is an extraordinary finding.

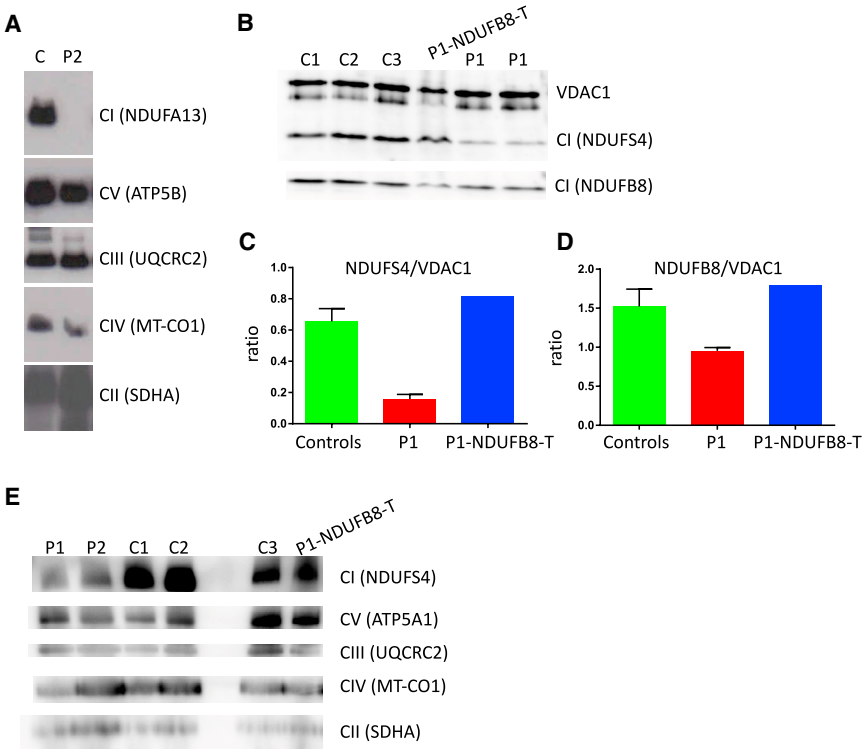

Figure 3. Biochemical Investigations in Fibroblasts

(A) Blue native gel electrophoresis of individual P2. Abbreviations: CI, complex I; CII, complex II; CIII, complex III; CIV, complex IV; CV, complex V; FCCP, carbonyl cyanide-4-(trifluoromethoxy)-phenylhydrazone.

(B) Western blot analysis of fibroblasts from individual P1, which were complemented by lentiviral transduction with wild-type *NDUFB8*. C1–C3 represent control fibroblasts. 10 μg protein were loaded. VDAC1 (porin) was used as a loading control. An antibody against the NDUFS4 subunit of complex I was used.

(C and D) Densitometric analysis of this western blot. Error bars indicate the standard error of the mean.

(E) Blue native gel electrophoresis of mitochondrial membranes prepared from fibroblasts of P1, P2, and controls solubilized by laurylmaltoside. Normalization of the complex I was observed after lentiviral transduction with wild-type *NDUFB8* (NDUFB8-T) in P1.

An aliquot of the PCR product was digested with the restriction enzyme BseYI (New England Biolabs), which cuts the wild-type PCR product twice (restriction sites on exon 3 and exon 4) but only once if the mutation c.432C>G is present on exon 4, resulting in labeled products of either 162 bases (c.432C, allele 1, wild-type and missense mutation at c.227A) or 321 bases (c.432G, allele 2-product a, missense mutation). Furthermore, a product of 165 bases (allele 2-product b, splice mutation) was found when exon 4 was missing in the transcript. Quantification of these three products results in 47% cDNA from allele 1, 14% cDNA from allele 2-product a, missense mutation, and 39% cDNA from allele 2-product b, splice defect (Figure S5). These investigations confirmed that the mutation c.432C>G predominantly results in a splice defect but also that a small amount of a transcript is detectable (14% of the whole cDNA) that contains the missense mutation leading to the predicted p.Cys144Trp exchange at the protein level.

The genetic defect in P2 was identified by targeted exome sequencing of a panel of 215 genes, including genes with known associations to mitochondrial disorders and genes of CI subunits and assembly factors. Sequencing was performed using DNA from peripheral blood as previously described.[17] From the 1,853 SNPs and indels identified in affected individual 2, we considered variants predicted to modify protein function (splice site, nonsense, missense, indels) of minor allele frequency less than 0.01 (for AR inheritance) in dbSNP, 1000 Genomes, ExAC, and Exome Variant Server and in our in-house project of 27,833 exomes of individuals with unrelated diseases. Bi-allelic filtering resulted in identification of one gene, *NDUFB8*. We detected two variants: (1) c.184T>C (p.Tyr62His) affecting a highly conserved amino acid of NDUFB8 on the paternally inherited allele and (2) a loss-of-function mutation c.189delA (p.Glu63Aspfs*35) on the maternally inherited allele of *NDUFB8* (Figure S7). All algorithms used for mutation prediction revealed high scores supporting pathogenic relevance (Table S1). None of the mutations was found in the ExAC and 1000 Genome databases. In the gnomAD database, two of the four variants were found: c.227C>A in 1/246,208 alleles and c.189delA in 3/244,804 alleles (Table S1).

In order to confirm that the CI deficiency was caused by *NDUFB8* variants, we performed functional complementation studies. The wild-type sequence of *NDUFB8* was amplified from a control cDNA and cloned into pLenti6.3/V5-TOPO TA Cloning Kit (Invitrogen) for expression of *NDUFB8* in human fibroblasts.[18,19] Transduced fibroblasts were investigated both enzymatically (P1) and by microscale respirometry (P1 and P2), western blotting (P1), flow cytometry analysis (P1), and immunohistochemical staining (P1 and P2). Since the complemented cells from P2 were not growing sufficiently well, not all investigations could be performed with complemented cells from both affected individuals.

The deficiency of respiratory chain complex I, measured in isolated mitochondria, was rescued after transduction of fibroblasts from P1 with wild-type *NDUFB8* (Table 1). Decreased basal and maximal respiration was found in fibroblasts of P1 and P2 as investigated by microscale respirometry (Seahorse), which returned to normal

Table 1. Activity of Oxidative Phosphorylation Enzymes in Fibroblasts of P1

Activity Normalized to Citrate Synthase	Complex I	Complex I+III	Complex II	Complex II+III	Complex III	Cytochrome *c* Oxidase	Oligomycin-Sensitive ATPase
P1 fibroblasts	0.02	0.23	0.43	1.00	2.48	1.73	1.02
P1 fibroblasts NDUFB8-Transduced	0.09	0.74	0.50	1.32	4.81	1.78	0.46
Reference range	0.04–0.12	0.23–0.53	0.18–0.43	0.29–0.69	0.72–2.23	0.9–1.79	0.39–0.79

activity after expression of wild-type NDUFB8 in both (Figure 4A).[19] Also, the amount of complex I protein normalized in NDUFB8 transduced fibroblasts as shown by western blot analysis on either SDS polyacrylamide electrophoresis with antibodies against NDUFS4 and NDUFB8 performed in P1 (Figures 3B–3D) or on blue native gel electrophoresis (Figure 3E).

Furthermore, fibroblasts of P1 and P2 were analyzed by flow cytometry. Fibroblasts (5×10^5 cells/well) were transferred in 100 μL 4% paraformaldehyde into a 96-well v-plate (Greiner Bio-One, Kremsmünster, Austria) and were fixed overnight. After centrifugation (300 × *g*, 4°C, 5 min), the cells were washed with 100 μL 1× PBS + 0.5% Tween-20 (PBS-T) (300 × *g*, 4°C, 5 min). The cell pellet was resuspended in 180 μL of 1 mmol/L EDTA, 0.05% Tween-20 (pH 8.0), transferred into PCR tubes, and heated in a thermo cycler at 95°C for 40 min. The cells were centrifuged, washed with PBS-T, and resuspended/incubated in 100 μL antibody diluent (with background reducing components) (Agilent) containing 1 μg/L × 10^6 cells primary antibody (complex I: anti-NDUFS4 (Abcam: ab137064); porin: anti-VDAC1 (Abcam: ab15895); isotype controls

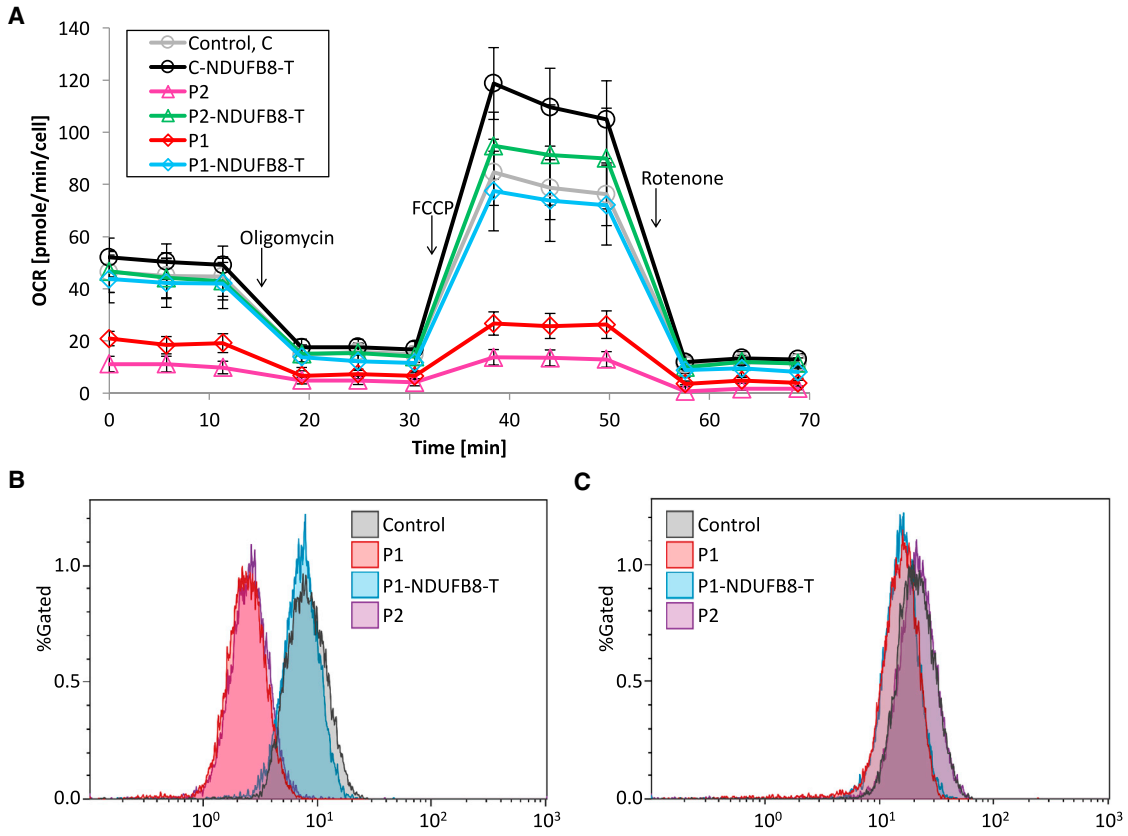

Figure 4. Microrespirometry and Flow Cytometry Analysis in Fibroblasts
(A) Oxygen consumption of fibroblasts of individual P1 and P2 compared to a control either with or without lentiviral transduction with wild-type *NDUFB8* (NDUFB8-T). At least 16 wells were analyzed per each sample, and at least two replicates were performed for each sample. Error bars indicate the standard deviation.
(B and C) Results of representative flow cytometry analysis of fibroblasts from individual P1, P1 transduced with wild-type *NDUFB8*, P2, and a control are shown. An antibody against the NDUFS4 subunit was used as marker for complex I (B), an antibody against VDAC1 (porin) as a control for mitochondria (C). Positive staining of primary antibodies was evaluated with suitable isotype controls. Mean fluorescence intensity (MFI) of complex I: Control = 8.59; P1 = 2.52; P1-NDUFB8-T = 7.59, P2 = 2.84. MFI of porin: Control = 22.15; P1 = 15.71; P1-NDUFB8 = 16.16, P2 = 22.36. Flow cytometry analysis of each sample was performed at least two times.

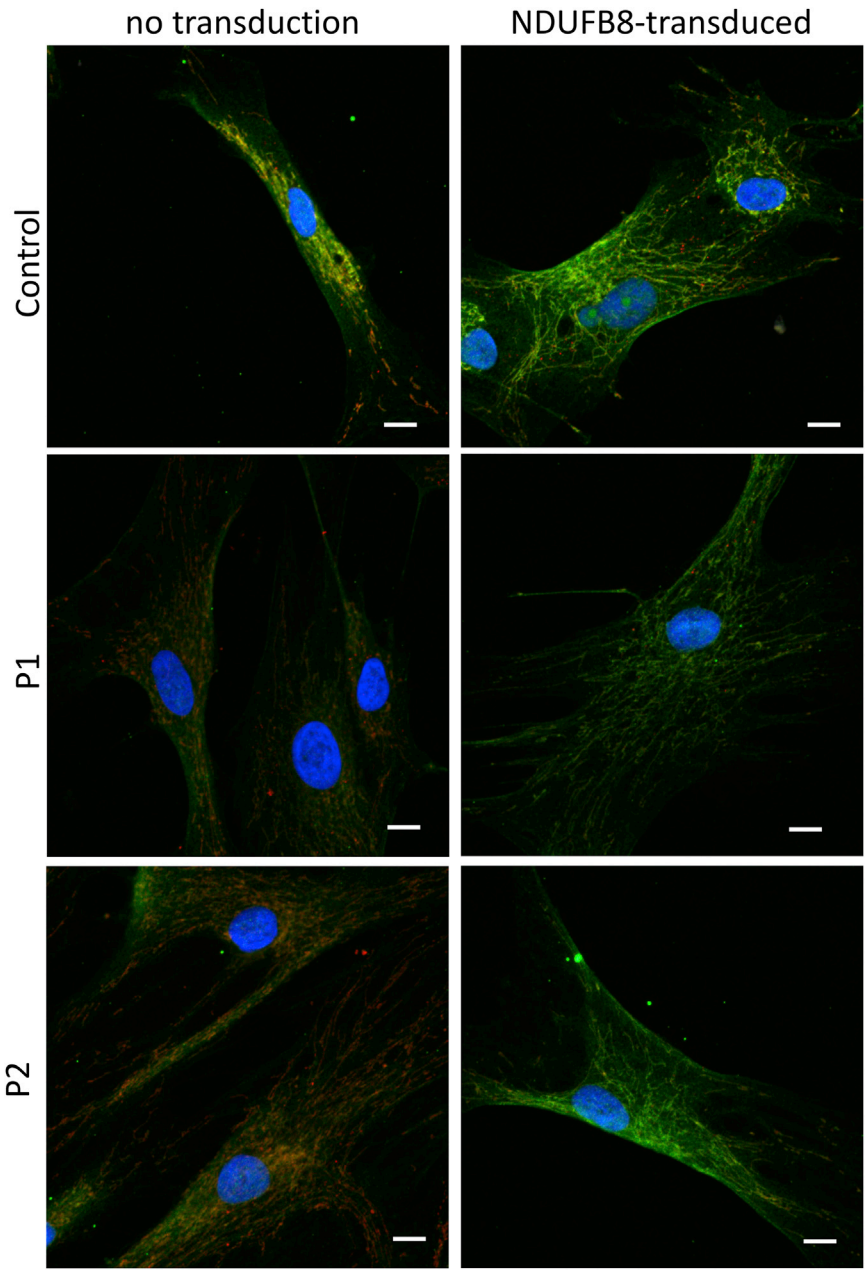

Figure 5. Immunofluorescence Staining of Complex I and Porin
Fibroblasts, transduced fibroblasts (NDUFB8-T) of individual P1, P2, and a control cell line were stained with antibodies against complex I subunit NDUFS4 (Abcam, 1:100) in green and VDAC1 (Abcam; 1:400), mitochondrial marker protein in red. The merge of staining is shown; all images were taken with the same microscope settings as used for the control (scale bar = 10 μm).

(Abcam: ab172730/Sigma-Aldrich: I5006) for 30 min at room temperature. The cells were washed with PBS-T and resuspended/incubated in 100 μL antibody diluent containing 2 μg/L × 10^6 cells secondary antibody (anti-rabbit IgG labeled with Alexa Fluor 488 [ThermoFisher: OR 97402]) for 30 min at room temperature. The pellet was washed with PBS-T and resuspended in flow cytometry staining buffer solution (ThermoFisher). Fluorescence was excited with a laser (488 nm) and the emission (519 nm) was detected via the FL1 channel by a flow cytometer (Cytomics FC 500 flow cytometer; Beckman Coulter). Data were analyzed (arithmetic mean) with Kaluza flow analyzing software 1.3 (Beckman Coulter). Fibroblasts from individual P1 and P2 showed a clear reduction of complex I compared to control fibroblasts (Figure 4B). In fibroblasts of P1 transduced with wild-type NDUFB8, a normalized amount of complex I was observed (Figure 4B).

Immunohistochemical staining was performed with fibroblasts of P1 and P2 compared to a control and revealed a decreased staining with a NDUFS4 antibody (Figures 5, S8, and S9).

Knowledge of the structure and function of human accessory subunits is constantly being expanded and derived mainly from *Yarrowia lipolytica* and *Bos taurus* structure models.[20,21] It was stated that ASHI, the bovine ortholog of human NDUFB8, is one of the accessory subunits encircling the core of CI and is bound to ND5 in the proton pumping module.[4] Recently solved 4.0-Å cryo-electron microscopy (cryo-EM) structure of the predominant supercomplex $CI_1III_2IV_1$ in porcine heart revealed direct contribution of the NDUFB8 in the oligomerization of CI, CIII, and CIV.[7] It is therefore conceivable that NDUFB8 damage entails strong cellular consequences demonstrated by severe phenotype of our two affected individuals.

The neuroradiological findings in both individuals with *NDUFB8* mutations were symmetrical basal ganglia and capsula interna lesions. P1 additionally showed progressive brain atrophy which may suggest that these lesions are broader than the classical Leigh syndrome lesions, the most frequent recognized phenotype in children with complex I deficiency.[8] As in a case with *NDUFAF2* defect and specific neuroimaging picture, this individual P1 demonstrates a subtype of LS with distinctive brain characteristics involving supratentorial brain lesions (Figure 2).[22] Given the small number of individuals with mutations in complex I accessory subunits or assembly factors, it is not possible to relate an individual

gene to a specific clinical phenotype.[23] Nevertheless, genotype-phenotype studies allow researchers to detect bilateral and symmetrical brainstem lesions as a common feature in complex I-deficient individuals.[24]

In conclusion, using next generation sequencing, we identified deleterious *NDUFB8* mutations in two complex I-deficient individuals. Complementation studies restored mitochondrial function, confirming a causal role of *NDUFB8* mutations in complex I deficiency. Our findings broaden the etiology of complex I deficiency and reveal NDUFB8 as an essential component for the stability and activity of complex I.

Supplemental Data

Supplemental Information includes Supplemental Note (case reports), nine figures, and one table and can be found with this article online at https://doi.org/10.1016/j.ajhg.2018.01.008.

Acknowledgments

The study was partly supported by NSC 2012/05/B/NZ2/01627 to D.P.-A., CMHI S136/13 and S145/16 to E.P., E-Rare project GENOMIT (01GM1603 and 01GM1207 to H.P., O1GML 1207 to A.R, Austrian Science Fonds [FWF]: I 2741-B26 to J.A.M.), PMU-FFF R-16/03/082-FEK (to R.G.F. and A.K.), and EC FP7-PEOPLE-ITN (GA #317433, MEET) projects.

Received: May 18, 2017
Accepted: January 11, 2018
Published: February 8, 2018

Web Resources

ExAC Browser, http://exac.broadinstitute.org/
GenBank, https://www.ncbi.nlm.nih.gov/genbank/
gnomAD Browser, http://gnomad.broadinstitute.org/
Human Splicing Finder 3.0, http://www.umd.be/HSF3/
Likelihood Ratio Test, http://www.genetics.wustl.edu/jflab/lrt_query.html
MutationTaster, http://www.mutationtaster.org/
OMIM, http://www.omim.org/
PolyPhen-2, http://genetics.bwh.harvard.edu/pph2/
SIFT, http://sift.bii.a-star.edu.sg/

References

1. Brandt, U. (2006). Energy converting NADH:quinone oxidoreductase (complex I). Annu. Rev. Biochem. *75*, 69–92.
2. Hirst, J. (2013). Mitochondrial complex I. Annu. Rev. Biochem. *82*, 551–575.
3. Lazarou, M., Thorburn, D.R., Ryan, M.T., and McKenzie, M. (2009). Assembly of mitochondrial complex I and defects in disease. Biochim. Biophys. Acta *1793*, 78–88.
4. Zhu, J., Vinothkumar, K.R., and Hirst, J. (2016). Structure of mammalian respiratory complex I. Nature *536*, 354–358.
5. Gu, J., Wu, M., Guo, R., Yan, K., Lei, J., Gao, N., and Yang, M. (2016). The architecture of the mammalian respirasome. Nature *537*, 639–643.
6. Letts, J.A., Fiedorczuk, K., and Sazanov, L.A. (2016). The architecture of respiratory supercomplexes. Nature *537*, 644–648.
7. Wu, M., Gu, J., Guo, R., Huang, Y., and Yang, M. (2016). Structure of mammalian respiratory supercomplex I1III2IV1. Cell *167*, 1598–1609.e10.
8. Fassone, E., and Rahman, S. (2012). Complex I deficiency: clinical features, biochemistry and molecular genetics. J. Med. Genet. *49*, 578–590.
9. Mayr, J.A., Haack, T.B., Freisinger, P., Karall, D., Makowski, C., Koch, J., Feichtinger, R.G., Zimmermann, F.A., Rolinski, B., Ahting, U., et al. (2015). Spectrum of combined respiratory chain defects. J. Inherit. Metab. Dis. *38*, 629–640.
10. Kremer, L.S., Bader, D.M., Mertes, C., Kopajtich, R., Pichler, G., Iuso, A., Haack, T.B., Graf, E., Schwarzmayr, T., Terrile, C., et al. (2017). Genetic diagnosis of Mendelian disorders via RNA sequencing. Nat. Commun. *8*, 15824.
11. Rodenburg, R.J. (2016). Mitochondrial complex I-linked disease. Biochim. Biophys. Acta *1857*, 938–945.
12. Haack, T.B., Haberberger, B., Frisch, E.M., Wieland, T., Iuso, A., Gorza, M., Strecker, V., Graf, E., Mayr, J.A., Herberg, U., et al. (2012). Molecular diagnosis in mitochondrial complex I deficiency using exome sequencing. J. Med. Genet. *49*, 277–283.
13. Haack, T.B., Danhauser, K., Haberberger, B., Hoser, J., Strecker, V., Boehm, D., Uziel, G., Lamantea, E., Invernizzi, F., Poulton, J., et al. (2010). Exome sequencing identifies ACAD9 mutations as a cause of complex I deficiency. Nat. Genet. *42*, 1131–1134.
14. Rustin, P., Chretien, D., Bourgeron, T., Gérard, B., Rötig, A., Saudubray, J.M., and Munnich, A. (1994). Biochemical and molecular investigations in respiratory chain deficiencies. Clin. Chim. Acta *228*, 35–51.
15. Pronicka, E., Piekutowska-Abramczuk, D., Ciara, E., Trubicka, J., Rokicki, D., Karkucińska-Więckowska, A., Pajdowska, M., Jurkiewicz, E., Halat, P., Kosińska, J., et al. (2016). New perspective in diagnostics of mitochondrial disorders: two years' experience with whole-exome sequencing at a national paediatric centre. J. Transl. Med. *14*, 174.
16. Olsen, R.K.J., Koňaříková, E., Giancaspero, T.A., Mosegaard, S., Boczonadi, V., Mataković, L., Veauville-Merllié, A., Terrile, C., Schwarzmayr, T., Haack, T.B., et al. (2016). Riboflavin-responsive and -non-responsive mutations in FAD synthase cause multiple acyl-CoA dehydrogenase and combined respiratory-chain deficiency. Am. J. Hum. Genet. *98*, 1130–1145.
17. Metodiev, M.D., Gerber, S., Hubert, L., Delahodde, A., Chretien, D., Gérard, X., Amati-Bonneau, P., Giacomotto, M.C., Boddaert, N., Kaminska, A., et al. (2014). Mutations in the tricarboxylic acid cycle enzyme, aconitase 2, cause either isolated or syndromic optic neuropathy with encephalopathy and cerebellar atrophy. J. Med. Genet. *51*, 834–838.
18. Kornblum, C., Nicholls, T.J., Haack, T.B., Schöler, S., Peeva, V., Danhauser, K., Hallmann, K., Zsurka, G., Rorbach, J., Iuso, A., et al. (2013). Loss-of-function mutations in MGME1 impair mtDNA replication and cause multisystemic mitochondrial disease. Nat. Genet. *45*, 214–219.
19. Kremer, L.S., and Prokisch, H. (2017). Identification of disease-causing mutations by functional complementation of patient-derived fibroblast cell lines. Methods Mol. Biol. *1567*, 391–406.
20. Vinothkumar, K.R., Zhu, J., and Hirst, J. (2014). Architecture of mammalian respiratory complex I. Nature *515*, 80–84.
21. Zickermann, V., Wirth, C., Nasiri, H., Siegmund, K., Schwalbe, H., Hunte, C., and Brandt, U. (2015). Structural biology.

Mechanistic insight from the crystal structure of mitochondrial complex I. Science *347*, 44–49.

22. Herzer, M., Koch, J., Prokisch, H., Rodenburg, R., Rauscher, C., Radauer, W., Forstner, R., Pilz, P., Rolinski, B., Freisinger, P., et al. (2010). Leigh disease with brainstem involvement in complex I deficiency due to assembly factor NDUFAF2 defect. Neuropediatrics *41*, 30–34.
23. Collet, M., Assouline, Z., Bonnet, D., Rio, M., Iserin, F., Sidi, D., Goldenberg, A., Lardennois, C., Metodiev, M.D., Haberberger, B., et al. (2016). High incidence and variable clinical outcome of cardiac hypertrophy due to ACAD9 mutations in childhood. Eur. J. Hum. Genet. *24*, 1112–1116.
24. Bricout, M., Grévent, D., Lebre, A.S., Rio, M., Desguerre, I., De Lonlay, P., Valayannopoulos, V., Brunelle, F., Rötig, A., Munnich, A., and Boddaert, N. (2014). Brain imaging in mitochondrial respiratory chain deficiency: combination of brain MRI features as a useful tool for genotype/phenotype correlations. J. Med. Genet. *51*, 429–435.